



Cyclic Deformation of Microcantilevers Using In-Situ Micromanipulation

Downloaded from: <https://research.chalmers.se>, 2026-04-04 12:54 UTC

Citation for the original published paper (version of record):

Harihara Subramonia Iyer, A., Hörnqvist Colliander, M. (2021). Cyclic Deformation of Microcantilevers Using In-Situ Micromanipulation. *Experimental Mechanics*, 61(9): 1431-1442. <http://dx.doi.org/10.1007/s11340-021-00752-3>

N.B. When citing this work, cite the original published paper.



Cyclic Deformation of Microcantilevers Using *In-Situ* Micromanipulation

A. H. S. Iyer¹ · M. H. Colliander¹

Received: 3 May 2021 / Accepted: 30 June 2021
© The Author(s) 2021

Abstract

Background The trend in miniaturisation of structural components and continuous development of more advanced crystal plasticity models point towards the need for understanding cyclic properties of engineering materials at the microscale. Though the technology of focused ion beam milling enables the preparation of micron-sized samples for mechanical testing using nanoindenters, much of the focus has been on monotonic testing since the limited 1D motion of nanoindenters imposes restrictions on both sample preparation and cyclic testing.

Objective/Methods In this work, we present an approach for cyclic microcantilever bending using a micromanipulator setup having three degrees of freedom, thereby offering more flexibility.

Results The method has been demonstrated and validated by cyclic bending of Alloy 718plus microcantilevers prepared on a bulk specimen. The experiments reveal that this method is reliable and produces results that are comparable to a nanoindenter setup.

Conclusions Due to the flexibility of the method, it offers straightforward testing of cantilevers manufactured at arbitrary position on bulk samples with fully reversed plastic deformation. Specific microstructural features, e.g., selected orientations, grain boundaries, phase boundaries etc., can therefore be easily targeted.

Keywords Micromechanics · Cyclic bending · Bauschinger effect · Micromanipulators · Electron microscopy

Introduction

Mechanical properties of materials often depend not only on the loading conditions, but also on load history, which is relevant for engineering materials since they frequently experience cyclic loading during service in many applications. It is therefore essential to evaluate and understand cyclic mechanical properties of materials, through which reliable life estimations can be performed. Fatigue of materials has been studied extensively over the past several decades, leading to standard methods being developed for fatigue testing and the mechanisms behind the phenomenon being understood [1]. However, with the trend in miniaturization of structural components, such as in MEMS applications, it is difficult to utilize standard testing methods to evaluate mechanical properties. Furthermore, the use of advanced

life estimation models requires inputs from the single crystal scale, which points toward the need for mechanical testing at micron level.

In response to these needs, recent developments in the areas of microscale mechanical testing equipment and focused ion beam (FIB) milling technology has made it possible to perform mechanical testing on microscale features [2, 3]. Specimen geometries such as microcantilevers [4, 5] and micropillars [6] have been tested in various studies using *in-situ* or *ex-situ* nanoindenters to evaluate mechanical properties of single grains [4, 7–10], grain boundaries [11–15], thin films [16–20], etc. Most of the studies have been focused on monotonic loading, and very few on cyclic loading since it is more complex. Some high cycle fatigue (HCF) studies at microscale has been carried out using continuous stiffness measurement (CSM) [21] technique, which involves the superposition of a small sinusoidal displacement during deformation. Merle et al. [22] used micropillar compression with 40 Hz CSM to perform HCF testing of ECAP copper to 3×10^6 cycles, and a similar study was conducted on bimodal copper laminates by Krauß et al. [23]. However,

✉ A. H. S. Iyer
harihara@chalmers.se

¹ Department of Physics, Chalmers University of Technology, Gothenburg, Sweden



for micropillar compression the load cycling is fully compressive, which does not necessarily translate to real conditions. Tensile loads can be achieved at the top surface of microcantilevers during bending, which was used by Merle et al. [24] to perform HCF tests for up to 3×10^6 cycles. As pre-loading was used to maintain contact between the tip and the sample during testing, the top surface remained in tension (positive stress ratio $R_\sigma = \sigma_{\min}/\sigma_{\max}$). Lavenstein et al. [25] used a nanoindenter with a tungsten probe attached to a microcantilever with SEM glue in order to perform fully reversed HCF testing of a superalloy, i.e. with $R_\sigma = -1$. For MEMS materials, high cycle fatigue studies at microscale have been performed through the use of micro-resonators [26, 27] and other special devices [28–30].

Reports of cyclic deformation with large scale reversed plasticity on the microscale, which is critical in order to understand phenomena like the Bauschinger effect and progressive fatigue damage evolution, are relatively scarce. The testing of microtensile specimens using *in-situ* nanoindenters with modified indenter tips have been carried out to study their fatigue properties [31, 32]. In a few studies microcantilevers have been used to investigate the cyclic deformation during reversed tensile/compressive cyclic loading [33, 34], including detailed Bauschinger effect analysis [35–37] and even fatigue crack propagation [33]. In the microcantilever bending studies, modified indentation tips with a claw-like opening were used to enable displacements to be applied in both directions. However, for most of these cases, especially cantilever bending, the specimens are made from thin rods/wires in order to allow the modified indenter tip to access the sample. This prohibits easy targeting of specific microstructural features in bulk polycrystalline specimens.

Having more degrees of freedom of motion for load application can greatly simplify testing configurations such as cyclic plastic bending. In this work, we present a method for cyclic microcantilever bending with full load reversal using a micromanipulator setup with three degrees of freedom. Such setups are typically used for manipulation of micron-sized features or in assisting TEM lamellae preparation, but here the unrestricted 3D motion is used to enable bending of microcantilevers in the surface plane of the bulk specimen from which they are prepared from, contrary to methods based on the use of nanoindenters which are only able to apply loads perpendicular to the surface plane. This allows testing of arbitrarily placed microcantilevers prepared on the surface of a bulk sample, enabling straightforward targeting of different features (such as phase, grain or twin boundaries) or orientations, as well as e.g., multiple cantilevers with different orientations in a single grain or single crystal. The flexibility offered by the system is a trade-off for stiffness and precision obtained from dedicated nanoindenters, as there is more room for error with micromanipulators. However, as will be shown, the accuracy is sufficient to allow

extraction of quantitative mechanical data during cyclic plastic bending.

Materials and Methods

Microcantilever Preparation

A nickel-based superalloy, Allvac 718plus, was selected as the material to demonstrate the principle of this cyclic deformation method. The surface of the sample was initially prepared by mechanical polishing using SiC abrasive papers up to 4000 grit, followed by broad ion beam (BIB) polishing for 6 h at 6.5 kV using 2.4 mA current. The sample was mounted on an aluminium stub using silver glue for microcantilever preparation. The microcantilevers were prepared using FEI Versa3D focused ion beam (FIB) microscope, on one of the edges of the specimen. It should be noted that this method does allow for preparation and testing of cantilevers prepared away from the edges as well, in which case they are of pentagonal cross-section which needs to be accounted for during data analysis. The choice of edge prepared cantilevers in this work is to simplify the post-test characterisation for validation of the method. The sample was mounted on a 45° pre-tilt holder so that milling can be performed on perpendicular faces of the sample without the need for remounting. The rough milling was performed using 15–30 nA current and the final polishing to obtain the geometry was performed at 100 pA current, and the beam energy was 30 keV for all steps. Near the fixed end of the microcantilever, a cross mark is made by electron deposition of platinum (10 keV, 0.52 nA), to track the total displacement during experiment. Towards the free end, 3 lines separated by $1 \mu\text{m}$ are milled across the width using an ion current of 10 pA to enable the tracking of cantilever displacement. The placement of the testing tip requires sufficient space around the microcantilever so that it does not touch the bulk material during experiment. Therefore, about $20 \mu\text{m}$ of material along the length direction and $10 \mu\text{m}$ on each side in width direction was removed during the rough milling steps. Figure 1 shows a finished microcantilever with markings. Electron



Fig. 1 Top view of a FIB milled microcantilever used for cyclic bending showing a platinum marker used for measuring load, and FIB-milled markers towards the free end used for tracking displacements

back scatter diffraction (EBSD) is performed on the prepared microcantilevers to determine their crystallographic orientation and to check for presence of grain boundaries along the cantilever length. Details regarding the dimensions of prepared microcantilevers is provided in section A of supplementary material.

Experimental Setup

In this work, MM3A micromanipulators from Kleindiek Nanotechnik GmbH are utilised for cyclic bending of microcantilevers. Some key specifications are included in Table 1. An image of the complete setup is provided in the supplementary material section B. However, the presented methodology is not reliant on a specific manipulator as long as the geometrical constraints imposed by the microscope and the force requirements resulting from the material/specimen geometry can be met. The micromanipulator arm has three degrees of freedom of movement (Fig. 2(a)), which provides the flexibility required for alignment and bending of microcantilevers in opposite directions. It also provides possibilities for different attachments as per requirements. The Kleindiek force measurement sensor (FMS), which is a piezoelectric sensor that measures force based on displacement of a probe in the form of a silicon cantilever, was used as the tip for testing (Fig. 2(e)). The FMS was chosen due to simplicity of modifying the shape using FIB, and also because it generates an audible feedback when in contact with a surface. It was not used for force measurement in this work since the range is limited ($\sim 360 \mu\text{N}$). However, the manipulators are flexible with respect to the type of attachment and any needle or similar probe can be used as long as a suitable tip geometry can be obtained.

The FMS tip was modified into the shape of a ‘claw’ with the use of FIB (Fig. 2(f)). The sensor was mounted on a 45° pre-tilt holder. Due to the geometry of FMS (where a protruding epoxy glue on the bottom side prevents from approaching the sample with the FMS cantilever parallel to the surface), it needs to approach the surface at an angle, as shown in Fig. 2(a). This implies that the claw has to be milled at an angle θ with respect to the horizontal, to ensure that the contact line is perpendicular to the length axis of the microcantilever during bending experiments, as shown

in the schematic in Fig. 2(d). As the cantilever must always be positioned in the electron beam path, and the manipulator is mounted in a fixed position in the chamber, the angle θ is decided by the working distance. In the current case, the angle was determined to be 13° for a working distance of 12 mm in the SEM. This value will depend on the setup used in the SEM chamber and can be varied depending on the working distance used, but remains a constant as long as the working distance or manipulator mounting does not change. Rough milling was performed at a current of 1 nA and the subsequent fine milling steps were performed at 100 pA current to obtain the final geometry. The beam energy was 30 keV for all the milling steps. The stage was tilted by an additional angle of 13° to mill the ‘claw’. The final geometry of the ‘claw’ used in the experiments is shown in Fig. 2(f), with a gap of about $4 \mu\text{m}$.

The force was measured using a dedicated spring table setup supplied by Kleindiek Nanotechnik GmbH. It consists of a spring of known spring constant, k , on which the sample can be mounted (Fig. 2(b)). Spring tables of various spring constants are available and is chosen based on the strength of the material being tested. During the bending experiment, SEM images are repeatedly acquired, which allows post-test evaluation of forces and displacements through image analysis. The spring moves along with the sample, and the displacement of the spring (measured by tracking the movement of a reference point on the sample) is used in measurement of force (Fig. 2(b)). The relative movement between a selected point on the microcantilever and the reference point is used for determining cantilever deflection. In Fig. 3, two images from before loading and at maximum load are compared, and the parameters used in force and displacement calculation are shown. The force is calculated as, $F = k \times \delta_I$, and the displacement is given by $\delta = \delta_2 - \delta_1$. The choice of spring table plays a role in the resolution of the data obtained. Low stiffness springs lead to larger displacements, thereby providing good resolution of force and displacement. But this can lead to a situation where it is not possible to achieve yielding without the cantilever moving out of the SEM image field. The force measurement requires a scan area that doesn’t move, as it is calculated from the absolute position of the marker, and therefore a spring is selected in such a way that yielding is achievable within the field of view at a certain magnification. The uncertainty of the spring constant values is within 5–10% according to the manufacturer.

Table 1 Key specifications of the Kleindiek MM3A micromanipulator used. Refer to Fig. 2 for definitions of the different axis of motion

	Φ_1	Φ_2	z
Operating range	240°	240°	12 mm
Maximum speed	10 mm s^{-1}	10 mm s^{-1}	2 mm s^{-1}
Resolution	$7 \times 10^{-9} \text{ rad}$ (0.5 nm)	$7 \times 10^{-9} \text{ rad}$ (0.2 nm)	$< 0.05 \text{ nm}$

Test Procedure

The Kleindiek micromanipulator setup is mounted on a Thermo Fischer FEI Quanta 200 FEG ESEM in such a way that relative motion between the stage and manipulator is possible. The sample is mounted on the spring table which

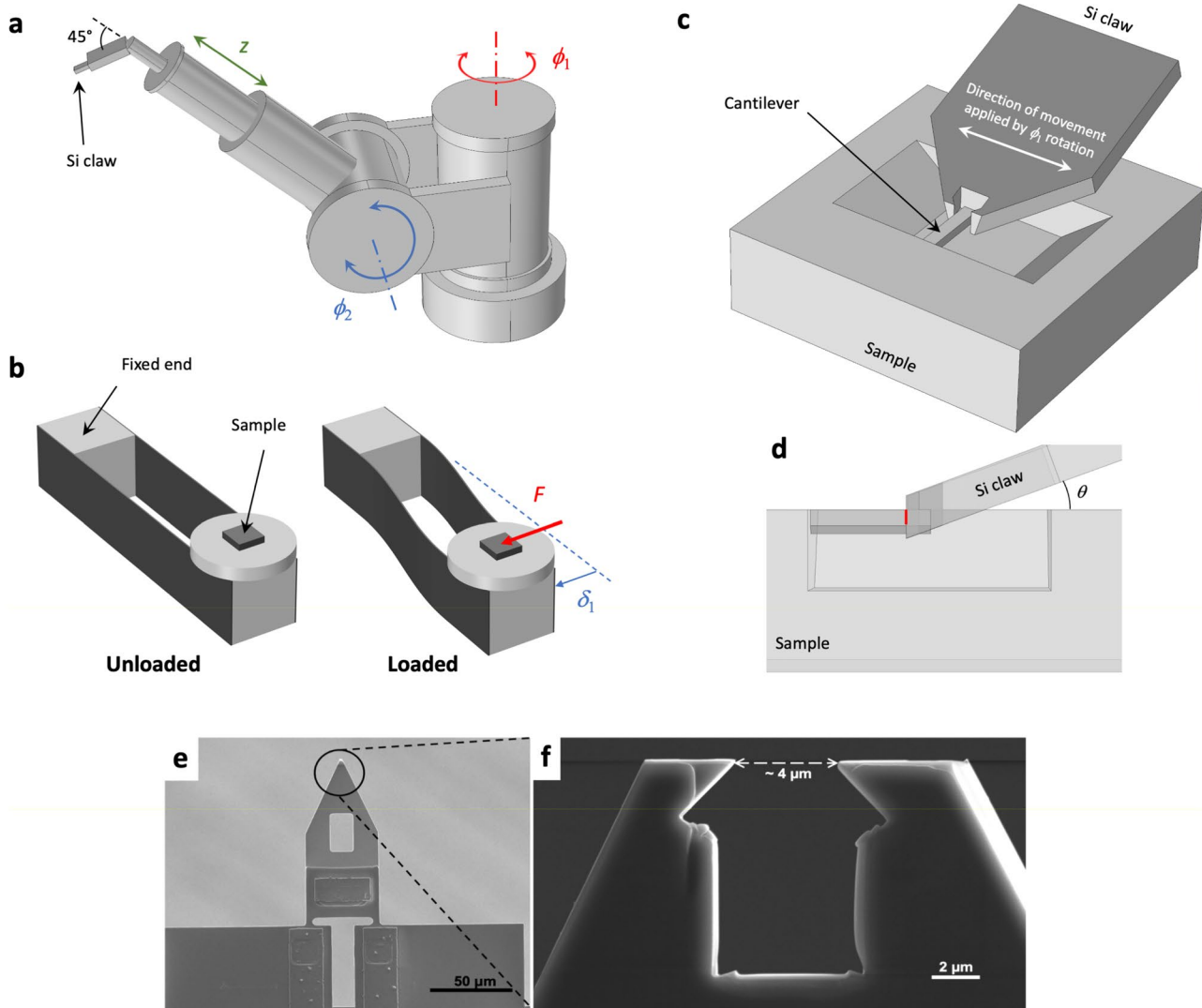


Fig. 2 (a) Schematic of Kleindiek micromanipulator used in this work with the rotation (ϕ_1 , ϕ_2) and translation (z) axes highlighted. The position of the silicon claw and its orientation is also shown; (b) Schematic of spring table showing how force measurement is performed. The blue and red arrows show the direction of displacement (δ) and force (F) respectively; (c) Orientation of the FIB milled sili-

con claw to the microcantilever is shown, where direction of loading is indicated as well; (d) a side view of (c) showing the alignment of the silicon claw with respect to the microcantilever to achieve line contact (indicated by the red line); (e) top view of the FMS as seen in SEM; and (f) The triangular shaped tip in (e) modified into a claw using FIB

is in turn mounted on the SEM stage. The FMS is then mounted on the manipulator arm so that there is an angle of 45° between the arm and the sensor to ensure that the FIB 'claw' can access the microcantilever without obstructions. As described above, the 45° angle together with a 12 mm working distance resulted in an angle between sample surface and the FMS cantilever of 13° in the setup used. The SEM stage is then rotated so that the free end of the microcantilever faces the FMS and the length axis of the cantilever and the arm are along the same line.

The setup is allowed to stabilise after reaching the desired vacuum level, until the drift rate is low enough

to have negligible impact on the force measurement. The position of the microcantilever to be tested is brought to the centre of field of view in the microscope through stage movement. The position of the micromanipulator arm is identified and it is moved towards the cantilever using the micromanipulator controls. The ϕ_2 and z axes motion are used to approach the sample surface. The image focus serves as a guide to determine how close the 'claw' is to the surface of the sample. With the current setup an audible feedback from the FMS control box denotes that contact has been established with the sample surface. The tip is carefully aligned in position using a combination



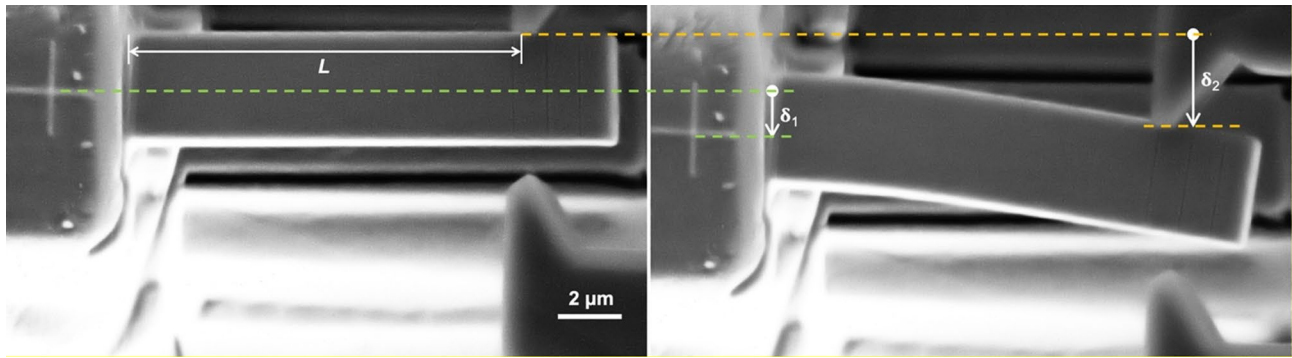


Fig. 3 SEM images of microcantilevers before (left) and after (right) loading. The green dotted line shows force measurement by image tracking (δ_1) and the orange dotted line shows the total displacement

of movements of ϕ_1 , ϕ_2 and z axes so that the testing can begin.

The testing is carried out using the movement along ϕ_1 axis (Fig. 2(a) and (c)) of the micromanipulator arm. The arm is moved along one direction to load the microcantilever beyond yielding. SEM images are recorded at a frequency of 1 Hz, which is later used for generating force–displacement curves, but the acquisition rate should be adjusted according to the applied deformation rate. After a complete half-cycle, i.e., reaching the maximum intended displacement and unloading, reverse bending of the microcantilever is performed by moving the micromanipulator in the opposite direction. About 3–4 cycles are repeated in such manner. The recorded SEM images are then analysed manually using a custom MATLAB script to extract the force–displacement data by tracking selected points on the sample and cantilever. The Pt mark shown in Fig. 1 is tracked to obtain the force (F) values for a cycle. While it would be possible to start the first cycle with the cantilever centred in field of view, which would then fit the full cycles, we started the deformation with the cantilever positioned close to the edge of the image opposite to the direction of movement. While this requires shifting the field of view between successive half-cycles, it allows a higher magnification, i.e., better resolution. Nevertheless, drift correction is applied by comparing the position of the Pt marker before and after the loading cycle and assuming linear drift (typical drift during a half-cycle was 100–150 nm during a time of 60–160 s). Each displacement measurement can then be corrected using the image time stamp and calculated linear drift rate. This is followed by tracking the loading tip at the point of contact with the microcantilever. This displacement in relation to the displacement of the Pt mark provides the cantilever displacement (δ). Thereafter, one of the displacement markers (Fig. 1) are tracked so that the cantilever displacement at a fixed span length (δ_{eq}) is known, which facilitates the comparison of different testing cycles for the same

of the loading point (δ_2). The span length (L) is the distance between the fixed end and point of contact (figure left)

microcantilever. For comparison of force between cycles, the force obtained from image analysis is converted into an equivalent force, F_{eq} using the equation, $F_{eq} = (F \times \delta) / \delta_{eq}$. The force–displacement curves were then converted to stress–strain curves to enable comparison of different cantilevers and to extract relevant mechanical properties. The bending stress (in the outer fibre) is calculated using the formula, $\sigma = (4FL) / (wh^2)$ [4, 36], where F is the force, L is the span length (Fig. 3 left), w and h are the width and height of the cantilever respectively. The surface strain is calculated using, $\epsilon = f \times (\delta / L)$, where δ is the displacement, and f is a scaling factor calculated using the radius of curvature of the cantilever at maximum displacement [36]. The details regarding this calculation are provided in supplementary material section C.

Results

Force–Displacement Response

Four microcantilevers were successfully tested for 3–4 cycles each for demonstrating the testing method and verifying its reliability. SEM images taken after cyclic bending tests clearly show the presence of plastic deformation (Fig. 4(a)) in the form of slip lines (Fig. 4(b)). Since the cantilevers have been deformed only for few cycles, no cracking or protrusion is expected. Cantilevers were also inspected from the side to verify the absence of out-of-plane deformation.

Figure 5 shows a representative force–displacement curve obtained after 4 cycles of forward and reverse loading of a microcantilever. The curves have been obtained after correction for drift and also compensating for gap between the claw and cantilever during a shift from forward to reverse loading. The residual displacement from previous cycles is added to the current cycle to obtain a continuous curve. As

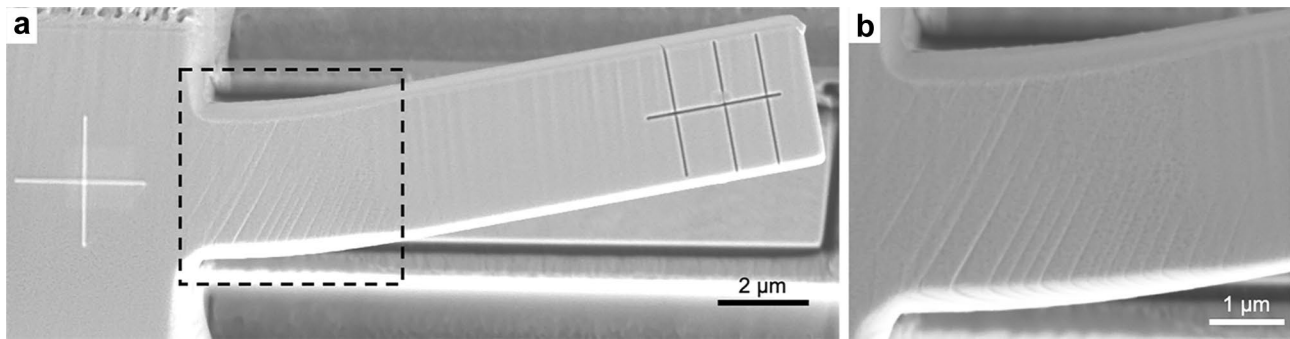


Fig. 4 (a) Top view SEM image of microcantilever O1 after testing; (b) highlighted region in (a) imaged at a higher magnification showing slip traces

mentioned before, the force and displacement resolution depend on the choice of the spring table. For the obtained data, the displacement resolution was obtained to be approximately 20 nm. Since the force is calculated directly from the displacement, for a spring table with stiffness of 1083 N/m, the force resolution is about 22 μN . In most cases, displacement for the first cycle was kept smaller in comparison with the following cycles to assess the elastic behaviour. In the following cycles, the microcantilever was bent beyond yield point during forward and reverse loading. During deformation the claw slides along the length of the microcantilever (which is accounted for when tracking the contact point), and therefore a constant span length and a corresponding equivalent force is used to compare and assemble different

half-cycles in an experiment using the formula in Sect. 2.3. For the given example in Fig. 5, the span length was kept at 10.6 μm .

Validation using Elastic Modulus Measurements

An estimation of elastic modulus was performed using the unloading slopes of force–displacement curves of tested microcantilevers. Prior to cyclic bending experiments, the cantilevers were subjected to elastic bending cycles using an Alemnis *in-situ* nanoindenter in a Zeiss Leo Ultra 55 FEG SEM. This was done so that the elastic modulus obtained from current method is comparable to that from a standard nanoindenter to estimate the reliability. It should be noted that here, the modulus has been used for a qualitative comparison rather than a quantitative, since microcantilever bending is not the best method to measure elastic modulus due to the strong geometric dependence. Fig. 6 shows the modulus values obtained from unloading slopes of the tested specimens using both nanoindenter and micromanipulator set ups (details are provided in section D of supplementary material). With the micromanipulator, an average value was calculated using the modulus obtained from unloading part of tested cycles and for the nanoindenter, multiple elastic bending tests were carried out by varying span lengths and then an average value was calculated from different curves for the same sample. It can be seen that the values for all four cantilevers are comparable between the two methods, and that the mechanical response obtained from the micromanipulator setup is therefore reliable. Single crystal elastic constants are not available for 718Plus, but for alloy 718, which has a very similar chemical composition, the elastic modulus varies between 113 GPa in $\langle 001 \rangle$ direction to 279 GPa in $\langle 111 \rangle$ according to theoretical calculations based on single crystal constants [38, 39]. In the present work, the modulus for O1, which is close to $\langle 001 \rangle$ has an average modulus of about 119 ± 15 GPa and N1 and N2, which are close to $\langle 111 \rangle$ have values of 261 ± 28 and 253 ± 18

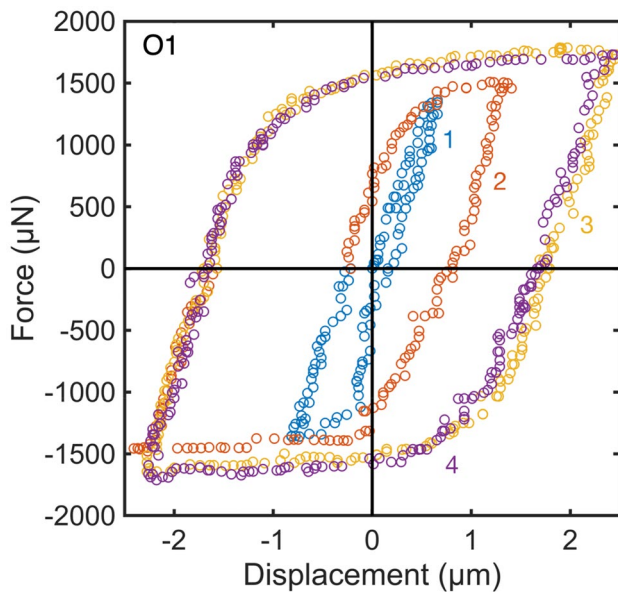


Fig. 5 Corrected force–displacement curve for a microcantilever (O1) showing 4 cycles (Note that there exists an uncertainty of 5–10% in the measured force levels). Coloured circles are used as markers to denote each cycle of loading



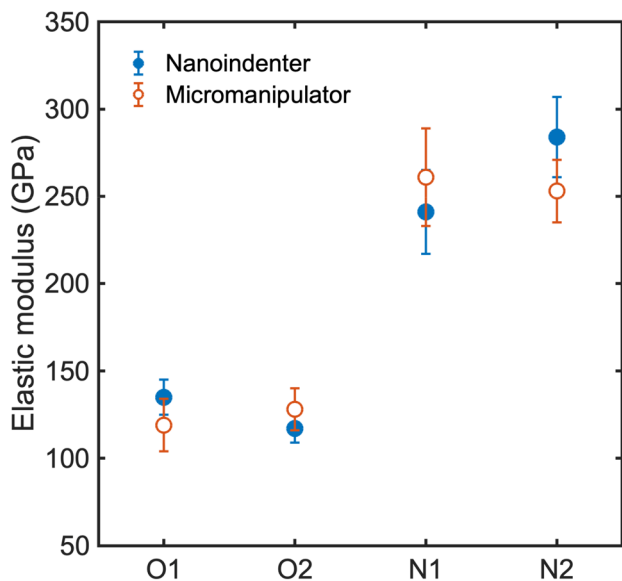


Fig. 6 Comparison of elastic modulus values from four different microcantilevers using nanoindenter (blue filled circle) and micromanipulator setup (brick red circle)

GPa, respectively, thereby showing good agreement with the expected values.

Stress–Strain Response

For comparing different cantilevers, and also to observe changes in plastic behaviour, the force–displacement curves were converted to stress–strain curves according to the previously outlined procedure. Fig. 7(a) shows the stress–strain curves calculated from F - δ data shown in Fig. 5. The sample has been bent to a maximum surface strain of ~6%, as seen in the final cycles from Fig. 7(a). In Fig. 7(b), two microcantilevers of different crystallographic orientations are compared using the calculated stress–strain curves. The difference in elastic modulus values between these two microcantilevers, as seen in Fig. 6 can also be inferred from the difference in unloading slopes of the stress–strain curves (dotted lines in Fig. 7(b)). The identical stress levels in the two orientations are a coincidence arising from the differences in strain history up to the displayed cycles. The stress levels in the first cycle (see Fig. 8) are higher in the N2 cantilever, which is expected due to the lower resolved shear stress of this orientation.

As mentioned in the introduction, one of the applications of this method is to study Bauschinger effect in single crystals during cyclic bending. Fig. 8 shows two examples where the forward and backward bending cycles have been shown on the same quadrant by inverting the signs of the reverse cycle, so that a comparison of yielding behaviour can be performed. The strains for the cycles have been added up

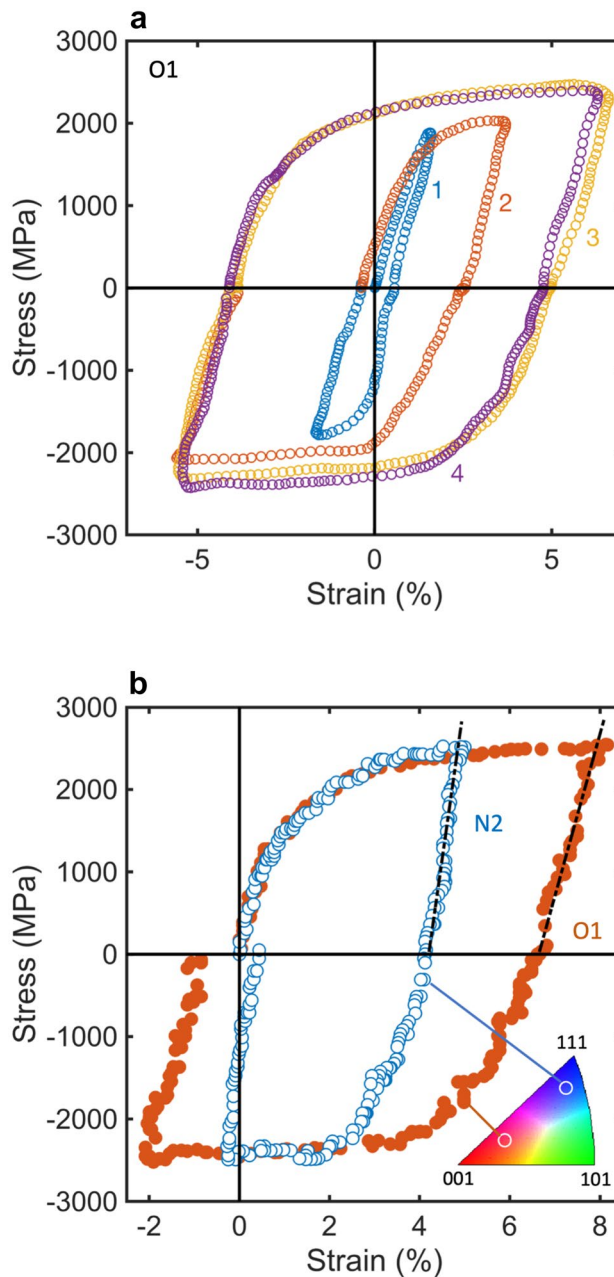


Fig. 7 (a) Stress–strain curves for O1 microcantilever showing 4 cycles – each cycle is shown with circles of different colour; **(b)** bending stress–strain curves for two cantilevers of different orientations (3rd cycle from sample N2 – blue circle, 4th cycle from sample O1 – filled brick red circle), shown in IPF along tensile direction. Note that an uncertainty of 5–10% in force measurement is also translated to the stress values

in the later cycles for demonstration purposes. The proof strength at 0.2% strain was used as a measure for qualitative comparison of yield behaviour between the cycles. For both cantilevers, the proof strength for reverse cycle is lower than that for the forward cycle. The decrease in proof strength is well beyond the uncertainty from force measurements.

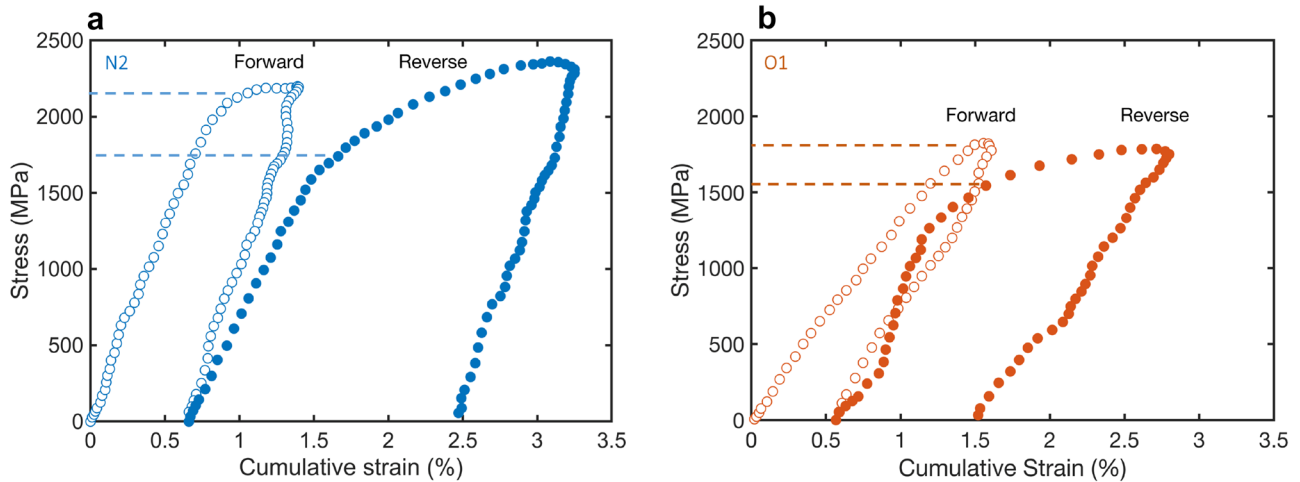


Fig. 8 Stress–strain curves demonstrating Bauschinger effect in two different microcantilevers (a) N2 and (b) O1 (forwards cycles represented by unfilled circles and reverse cycle by filled circles)

Such a yielding behaviour indicates Bauschinger effect in the tested 718plus single crystals.

Accuracy

To examine the accuracy of the method two microcantilevers were prepared from the same grain of the material. One was tested with the nanoindenter setup monotonically and the other cyclically using micromanipulator setup. Although the loading directions are different (perpendicular to each other) for the two setups, the mechanical response is not influenced since the material has a cubic crystal structure. The cantilever tested with nanoindenter setup was tested in several stages in displacement control mode. Initially, the specimen was bent elastically with 200 and 500 nm displacement in order to estimate the elastic modulus, followed by a displacement of $\sim 1.5 \mu\text{m}$ to bend it plastically. Cyclic bending of the other microcantilever in the same grain was conducted for 4 cycles using the micromanipulator setup. The comparison of stress–strain curves from the first cycle with the data obtained from the plastic bending using the nanoindenter suggests that there is reasonable agreement between the mechanical response from the two microcantilevers in the same grain, tested with the two methods (see Fig. 9). The elastic modulus from the microcantilever tested using nanoindenter was $108 \pm 5 \text{ GPa}$ and that from micromanipulator tested microcantilever was $119 \pm 15 \text{ GPa}$, which also shows reasonable agreement with each other.

Repeatability

The repeatability was tested by bending of microcantilevers prepared in the same grain. Fig. 10 shows comparison

of half cycles from cyclic bending experiments, where it can be seen that the mechanical behaviour is very similar for the two microcantilevers. The maximum displacement for the microcantilevers were different, leading to different bending and residual strains. Both elastic and plastic part of the curves are in agreement for the microcantilevers, and therefore it can be said that the results obtained using this test setup are repeatable.

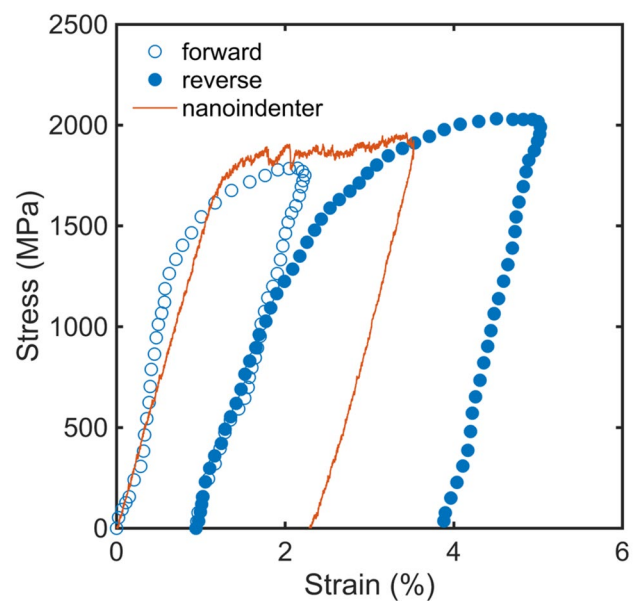


Fig. 9 Stress–strain curves comparing mechanical response of microcantilevers in the same grain tested using both setups. For the micromanipulator setup, there is an uncertainty of 5–10% in stress (line – nanoindenter, unfilled blue circle for forward cycle of micromanipulator and its reverse cycle is represented with filled blue circles)



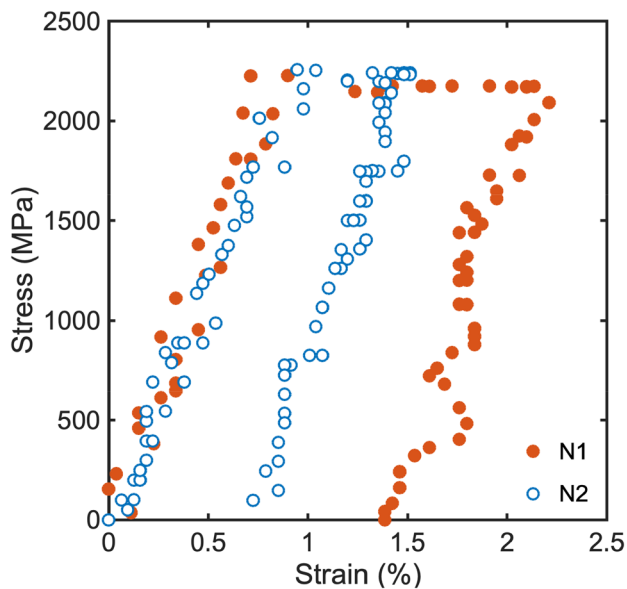


Fig. 10 Mechanical behaviour of microcantilevers N1 (unfilled blue circles) and N2 (filled brick red circles) belonging to the same grain. Stress level uncertainty is 5–10%

Discussion

Cyclic microcantilever bending using micromanipulators simplifies the process of sample preparation and expands the range of applications as it removes the need for modification of the sample into rods or wires. In this work, it has been clearly demonstrated that cyclic bending of microcantilevers is possible with slight modifications of an existing micromanipulator setup. The method is reliable and the results are comparable to those obtained from a standard nanoindenter. This has been demonstrated through elastic modulus measurements of tested specimens using the current setup as well as an *in-situ* nanoindenter, which shows that the measurements are within the limits of error of each other, and are in agreement with literature values. Additionally, it has been established that the complete elastic–plastic mechanical response generated from both setups are comparable and the repeatability of the setup has been shown through testing multiple cantilevers prepared in the same grain of the material. As demonstrated here, this method enables study of the Bauschinger effect and similar phenomenon where fully reversible loading is necessary.

However, the use of micromanipulators for micromechanical experiments comes with certain issues which needs careful attention:

- In comparison to dedicated nanoindenters, which are rigid in all directions apart from loading direction, the current system is not as stable. This leads to a decreased

level of accuracy and precision which should be carefully analysed and addressed for the specific set-up used.

- Unlike nanoindenters, the motion of micromanipulators (and the sample) is not in a straight line but an arc. Since the displacements are very small in comparison to the total length of the manipulator arm, the resulting displacement perpendicular to the intended direction of motion is of the same order as the displacement resolution and therefore can be neglected. Even in situations where the perpendicular displacement would become noticeable, this can be handled by the continuous tracking of the contact point between the 'claw' and the cantilever and the reference point on the sample. As the design of the spring table ensures that there is no rotation of the sample when the spring bends (see Fig. 2) the correct span length can be determined at each point of the test. Furthermore, since only the vertical part of the movement of the reference point is considered in the force calculations, the resulting force values are not affected by the perpendicular displacement.
- The spring table used in force measurements have an uncertainty of about 5–10% according to the manufacturer, and this needs to be taken into account when representing force in measurements. Separate calibration experiments using samples with precisely known stiffness can be used to reduce this uncertainty if needed.

Furthermore, there are some issues specific to the application of micromanipulators for cyclic testing:

- The alignment of the claw with the cantilever is an important factor to take into account. The contact points on both sides of the cantilever should be as parallel as possible and cover the height of the cantilever to ensure a proper line contact, as any tilting can cause the cantilever to twist or bend in the perpendicular direction of loading. Such an alignment is performed in this work using the top-view SEM image of the claw, which can indicate whether it is tilted or not.
- The line of contact should be as perpendicular to the sample surface as possible for accurate determination of span length. Once θ is determined for a certain working distance, the contact can be verified just through the use of SEM images of the claw during testing.

In addition to above, geometrical inaccuracies in cantilever and claw preparation can also affect the accuracy of the results produced. This is however, an issue when conducting any experiments using FIB prepared specimens and can only be solved through careful optimisation of milling parameters that can limit both geometrical issues and gallium damage.

The quality of data obtained from the proposed setup could be further increased through an increased sampling

rate, which is limited in this case by the frequency of acquisition of SEM images of sufficient quality for reliable analysis, and the spring constant of the selected spring table. A higher sampling rate, slower loading rate or a softer spring would provide more data points. However, the current setup utilises manual loading, which makes it difficult to tune the loading rate precisely. Also, lowering the rate of loading would increase the time for a cycle and hence increases drift issues. Since the computer interface allows scripting, there is a possibility to control the motion of the micromanipulator arm more precisely. However, since the actuators on the current manipulator are not encoded, the range of movement needs to be determined for each situation (new version of the specific manipulator used here do, however, include position encoded piezo actuators). The use of scripting also removes another main limitation of the current setup, which is the number of loading cycles that can be carried out in a reasonable amount of time. Since the loading is manual and the number of data points obtained is limited to 1 Hz, a large number of cycles could take several hours to days. Automation of the loading process through scripting, and the use of a screen grabbing software for recording images at the highest SEM scanning rates possible could significantly increase the maximum number of cycles.

Although not explored in the current study, which is aimed at demonstrating the use of micromanipulators for realization of cyclic plastic bending of microcantilevers, the visual access to the top surface of the cantilever offers a possibility to study development of strain gradients in more detail. If e.g. a Pt speckle pattern [40] is deposited close to the fixed end before testing, high resolution imaging at maximum load or between the half cycles would allow extraction of the (residual) strain field development during cycling using digital image correlation (DIC) [41]. Depending on whether or not sufficient stability can be achieved, which would likely depend on the details of both sample material and test setup, imaging for DIC extraction of strain fields could even be performed during loading (although this would have to be done without exact knowledge of the force since switching between a high magnification view of the speckle pattern and a low magnification view of the cantilever for displacement tracking would lead to a loss in the precision of the absolute displacement of the reference point). As the geometry at the fixed end can easily be modified, this could allow e.g., different notch geometries to be used and compared.

Conclusions

A new method for *in-situ* cyclic plastic deformation of microcantilevers inside SEMs based on use of micromanipulators combined with spring table based force measurement has

been demonstrated in this work. This new approach enables application of arbitrary reversed bending cycles with large levels of plasticity, as well as targeting various microstructural features directly from bulk samples without the need for modifications into rods or wires. Validation experiments performed using single crystal microcantilevers manufactured from a polycrystalline Ni-base superalloy bulk sample clearly demonstrate that the method produces results consistent with standard nanoindenters. Elastic modulus values measured using the setup show good agreement with both literature and control measurements using a nanoindenter. The accuracy and repeatability of the measured cyclic stress–strain response has been shown through specific experiments. An additional benefit of the method is the comparatively low cost of a micromanipulator/spring table setup, which makes cyclic plastic testing accessible to a larger community.

Supplementary Information The online version contains supplementary material available at <https://doi.org/10.1007/s11340-021-00752-3>.

Acknowledgements This work was funded by the Swedish Foundation for Strategic research under grant number ITM17-0003. The work was performed in part at the Chalmers Material Analysis Laboratory, CMAL.

Funding Open access funding provided by Chalmers University of Technology.

Declarations

Conflict of Interest This work was funded by the Swedish Foundation for Strategic research under grant number ITM17-0003. The authors have no conflicts of interest to declare that are relevant to the content of this article.

Open Access This article is licensed under a Creative Commons Attribution 4.0 International License, which permits use, sharing, adaptation, distribution and reproduction in any medium or format, as long as you give appropriate credit to the original author(s) and the source, provide a link to the Creative Commons licence, and indicate if changes were made. The images or other third party material in this article are included in the article's Creative Commons licence, unless indicated otherwise in a credit line to the material. If material is not included in the article's Creative Commons licence and your intended use is not permitted by statutory regulation or exceeds the permitted use, you will need to obtain permission directly from the copyright holder. To view a copy of this licence, visit <http://creativecommons.org/licenses/by/4.0/>.

References

1. Suresh S (1998) Fatigue of Materials. Cambridge University Press
2. Dehm G, Jaya BN, Raghavan R, Kirchlechner C (2018) Overview on micro- and nanomechanical testing: New insights in interface plasticity and fracture at small length scales. Acta Mater 142:248–282. <https://doi.org/10.1016/j.actamat.2017.06.019>
3. Ast J, Ghidelli M, Durst K et al (2019) A review of experimental approaches to fracture toughness evaluation at the micro-scale. Mater Des 173:107762. <https://doi.org/10.1016/j.matdes.2019.107762>



4. Motz C, Schöberl T, Pippan R (2005) Mechanical properties of micro-sized copper bending beams machined by the focused ion beam technique. *Acta Mater* 53:4269–4279. <https://doi.org/10.1016/j.actamat.2005.05.036>
5. Di Maio D, Roberts SGG (2005) Measuring fracture toughness of coatings using focused-ion-beam-machined microbeams. *J Mater Res* 20:299–302. <https://doi.org/10.1557/JMR.2005.0048>
6. Uchic MD (2004) Sample Dimensions Influence Strength and Crystal Plasticity. *Science* (80-) 305:986–989. <https://doi.org/10.1126/science.1098993>
7. Iqbal F, Ast J, Göken M, Durst K (2012) *In situ* micro-cantilever tests to study fracture properties of NiAl single crystals. *Acta Mater* 60:1193–1200. <https://doi.org/10.1016/j.actamat.2011.10.060>
8. Henry R, Blay T, Douillard T et al (2019) Local fracture toughness measurements in polycrystalline cubic zirconia using micro-cantilever bending tests. *Mech Mater* 136:103086. <https://doi.org/10.1016/j.mechmat.2019.103086>
9. Norton AD, Falco S, Young N et al (2015) Microcantilever investigation of fracture toughness and subcritical crack growth on the scale of the microstructure in Al₂O₃. *J Eur Ceram Soc* 35:4521–4533. <https://doi.org/10.1016/j.jeurceramsoc.2015.08.023>
10. Montagne A, Pathak S, Maeder X, Michler J (2014) Plasticity and fracture of sapphire at room temperature: Load-controlled micro-compression of four different orientations. *Ceram Int* 40:2083–2090. <https://doi.org/10.1016/j.ceramint.2013.07.121>
11. Dugdale H, Armstrong DEJ, Tarleton E et al (2013) How oxidized grain boundaries fail. *Acta Mater* 61:4707–4713. <https://doi.org/10.1016/j.actamat.2013.05.012>
12. Armstrong DEJ, Wilkinson AJ, Roberts SG (2011) Micro-mechanical measurements of fracture toughness of bismuth embrittled copper grain boundaries. *Philos Mag Lett* 91:394–400. <https://doi.org/10.1080/09500839.2011.573813>
13. Kupka D, Lilleodden ET (2011) Mechanical Testing of Solid-Solid Interfaces at the Microscale. *Exp Mech* 52:649–658. <https://doi.org/10.1007/s11340-011-9530-z>
14. Ast J, Göken M, Durst K (2017) Size-dependent fracture toughness of tungsten. *Acta Mater* 138:198–211. <https://doi.org/10.1016/j.actamat.2017.07.030>
15. Kupka D, Huber N, Lilleodden ETT (2014) A combined experimental-numerical approach for elasto-plastic fracture of individual grain boundaries. *J Mech Phys Solids* 64:455–467. <https://doi.org/10.1016/j.jmps.2013.12.004>
16. Matoy K, Schönherr H, Detzel T et al (2009) A comparative micro-cantilever study of the mechanical behavior of silicon based passivation films. *Thin Solid Films* 518:247–256. <https://doi.org/10.1016/j.tsf.2009.07.143>
17. Iyer AHS, Stiller K, Colliander MH (2018) Room temperature plasticity in thermally grown sub-micron oxide scales revealed by micro-cantilever bending. *Scr Mater* 144:9–12. <https://doi.org/10.1016/j.scriptamat.2017.09.036>
18. Konetschnik R, Daniel R, Brunner R, Kiener D (2017) Selective interface toughness measurements of layered thin films. *AIP Adv* 7. <https://doi.org/10.1063/1.4978337>
19. Soler R, Gleich S, Kirchlechner C et al (2018) Fracture toughness of Mo₂BC thin films: Intrinsic toughness versus system toughening. *Mater Des* 154:20–27. <https://doi.org/10.1016/j.matdes.2018.05.015>
20. Sebastiani M, Johanns KE, Herbert EG et al (2015) A novel pillar indentation splitting test for measuring fracture toughness of thin ceramic coatings. *Philos Mag* 95:1928–1944. <https://doi.org/10.1080/14786435.2014.913110>
21. Oliver WC, Pethica JB (1989) Method for continuous determination of the elastic stiffness of contact between two bodies. *US Pat* 4:141
22. Merle B, Höppel HW (2018) Microscale High-Cycle Fatigue Testing by Dynamic Micropillar Compression Using Continuous Stiffness Measurement. *Exp Mech* 58:465–474. <https://doi.org/10.1007/s11340-017-0362-3>
23. Krauß S, Schieß T, Göken M, Merle B (2020) Revealing the local fatigue behavior of bimodal copper laminates by micropillar fatigue tests. *Mater Sci Eng A* 788. <https://doi.org/10.1016/j.msea.2020.139502>
24. Gabel S, Merle B (2020) Small-scale high-cycle fatigue testing by dynamic microcantilever bending. *MRS Commun* 10:332–337. <https://doi.org/10.1557/mrc.2020.31>
25. Lavenstein S, Crawford B, Sim GD et al (2018) High frequency *in situ* fatigue response of Ni-base superalloy René-N5 microcrystals. *Acta Mater* 144:154–163. <https://doi.org/10.1016/j.actamat.2017.10.049>
26. Muhlstein CL, Brown SB, Ritchie RO (2001) High-Cycle Fatigue of Polycrystalline Silicon Thin Films in Laboratory Air. C. L. Muhlstein *, S.B. Brown †, and R.O. Ritchie *. *Mater Res* 657:1–6
27. Barrios A, Gupta S, Castelluccio GM, Pierron ON (2018) Quantitative *in Situ* SEM High Cycle Fatigue: The Critical Role of Oxygen on Nanoscale-Void-Controlled Nucleation and Propagation of Small Cracks in Ni Microbeams. *Nano Lett* 18:2595–2602. <https://doi.org/10.1021/acs.nanolett.8b00343>
28. Hommel M, Kraft O, Arzt E (1999) A new method to study cyclic deformation of thin films in tension and compression. *J Mater Res* 14:2373–2376. <https://doi.org/10.1557/JMR.1999.0317>
29. Zhang H, Jiang C, Lu Y (2017) Low-Cycle Fatigue Testing of Ni Nanowires Based on a Micro-Mechanical Device. *Exp Mech* 57:495–500. <https://doi.org/10.1007/s11340-016-0199-1>
30. Qi M, Liu Z, Yan X (2014) A low cycle fatigue test device for micro-cantilevers based on self-excited vibration principle. *Rev Sci Instrum* 85:1–6. <https://doi.org/10.1063/1.4898668>
31. Huang K, Sumigawa T, Kitamura T (2020) Load-dependency of damage process in tension-compression fatigue of microscale single-crystal copper. *Int J Fatigue* 133:105415. <https://doi.org/10.1016/j.ijfatigue.2019.105415>
32. Sumigawa T, Uegaki S, Yukishita T et al (2019) FE-SEM *in situ* observation of damage evolution in tension-compression fatigue of micro-sized single-crystal copper. *Mater Sci Eng A* 764:138218. <https://doi.org/10.1016/j.msea.2019.138218>
33. Howard C, Fritz R, Alfreider M et al (2017) The influence of microstructure on the cyclic deformation and damage of copper and an oxide dispersion strengthened steel studied via *in-situ* micro-beam bending. *Mater Sci Eng A* 687:313–322. <https://doi.org/10.1016/j.msea.2017.01.073>
34. Kiener D, Motz C, Grosinger W et al (2010) Cyclic response of copper single crystal micro-beams. *Scr Mater* 63:500–503. <https://doi.org/10.1016/j.scriptamat.2010.05.014>
35. Eisenhut L, Schaefer F, Gruenewald P et al (2017) Effect of a dislocation pile-up at the neutral axis on trans-crystalline crack growth for micro-bending fatigue. *Int J Fatigue* 94:131–139. <https://doi.org/10.1016/j.ijfatigue.2016.09.015>
36. Demir E, Raabe D (2010) Mechanical and microstructural single-crystal Bauschinger effects: Observation of reversible plasticity in copper during bending. *Acta Mater* 58:6055–6063. <https://doi.org/10.1016/j.actamat.2010.07.023>
37. Kapp MW, Kirchlechner C, Pippan R, Dehm G (2015) Importance of dislocation pile-ups on the mechanical properties and the Bauschinger effect in microcantilevers. *J Mater Res* 30:791–797. <https://doi.org/10.1557/jmr.2015.49>
38. Kumara C, Deng D, Moverare J, Nylén P (2018) Modelling of anisotropic elastic properties in alloy 718 built by electron beam melting. *Mater Sci Technol (United Kingdom)* 34:529–537. <https://doi.org/10.1080/02670836.2018.1426258>
39. Martin G, Ochoa N, Saï K et al (2014) A multiscale model for the elastoviscoplastic behavior of Directionally Solidified alloys: Application to FE structural computations. *Int J Solids Struct* 51:1175–1187. <https://doi.org/10.1016/j.ijsolstr.2013.12.013>
40. Di Gioacchino F, Clegg WJ (2014) Mapping deformation in small-scale testing. *Acta Mater* 78:103–113. <https://doi.org/10.1016/j.actamat.2014.06.033>



41. Edwards TEJ, Di Gioacchino F, Mohanty G et al (2018) Longitudinal twinning in a TiAl alloy at high temperature by *in situ* microcompression. Acta Mater 148:202–215. <https://doi.org/10.1016/j.actamat.2018.01.007>

Publisher's Note Springer Nature remains neutral with regard to jurisdictional claims in published maps and institutional affiliations.

